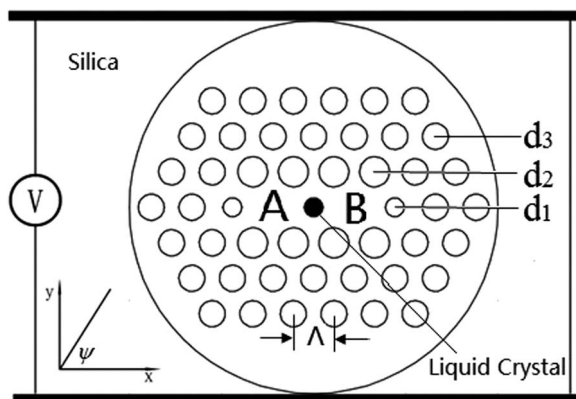


# A Novel Polarization Splitter Based on Dual-Core Photonic Crystal Fiber With a Liquid Crystal Modulation Core

Volume 6, Number 4, August 2014

H. L. Chen  
S. G. Li  
Z. K. Fan  
G. W. An  
J. S. Li  
Y. Han



---

DOI: 10.1109/JPHOT.2014.2337874  
1943-0655 © 2014 IEEE

# A Novel Polarization Splitter Based on Dual-Core Photonic Crystal Fiber With a Liquid Crystal Modulation Core

H. L. Chen, S. G. Li, Z. K. Fan, G. W. An, J. S. Li, and Y. Han

Key Laboratory of Metastable Materials Science and Technology, College of Science, Yanshan University, Qinhuangdao, 066004, China

DOI: 10.1109/JPHOT.2014.2337874

1943-0655 © 2014 IEEE. Translations and content mining are permitted for academic research only.  
Personal use is also permitted, but republication/redistribution requires IEEE permission.  
See [http://www.ieee.org/publications\\_standards/publications/rights/index.html](http://www.ieee.org/publications_standards/publications/rights/index.html) for more information.

Manuscript received May 5, 2014; revised June 30, 2014; accepted July 1, 2014. Date of publication July 10, 2014; date of current version July 24, 2014. This work was supported in part by the National Natural Science Foundation of China under Grant 61178026 and in part by the Natural Science Foundation of Hebei Province, China, under Grant E2012203035. Corresponding Author: H. Chen (e-mail: hlchen@ysu.edu.cn).

**Abstract:** A novel polarization splitter based on dual-core silica glass photonic crystal fiber with a liquid crystal modulation core is studied by the finite-element method. The mode birefringence is enlarged greatly with the infilling of nematic liquid crystal of E7. The simulation results demonstrate that the polarization splitter has an ultrabroad bandwidth of 250 nm, covering the E S C L optical communication bands, with the extinction ratio better than  $-20$  dB. The separate length is 0.175 mm, and the extinction ratio is  $-80.7$  dB at the communication wavelength of 1550 nm. The polarization splitter exhibits satisfactory splitter performance as the fabrication deviation reaches to 1%. The extinction ratio maintains better than  $-20$  dB, at the C L optical communication bands, as the temperature increases from  $15^{\circ}\text{C}$  to  $50^{\circ}\text{C}$ .

**Index Terms:** Photonic crystal fiber, Beam splitters, Liquid crystal.

## 1. Introduction

Photonic Crystal Fibers (PCFs), infiltrated with functional materials effectively combining the holey micro structure with the physical performance of the materials, have been a promising investigation field in photonic devices [1]–[3]. The functional materials infilling in the photonic crystal fibers show various physical effects under different external fields. Surface plasmon resonance excited by the infilling of metal wires [4], films [5] and nano-particles solutions [6] in PCFs has been used to fabricate sensors with high sensitivity. The magnetic nano-particles solutions sensitivity to the external temperature, electrical field and magnetic field were infiltrated in the photonic devices [7]. The solutions of thermo-optical effect, such as toluene, alcohol, chloroform and the mixture were infiltrated in the fiber air holes to obtain a high sensitivity temperature sensor [8]–[10]. The liquid crystal which is sensitive to the temperature and electrical field has been widely used to fabricate photonic functional devices in recent years [11]. Arc-fusion techniques [12] were successfully implemented for the liquid infiltration of air holes. The photonic bandgap silica PCFs infiltrated with liquid crystal have been experimentally shown in [13], [14]. The anisotropic material of nematic liquid crystal (NLC) of E7 infiltrated in the air holes of a soft glass PCF produces a big birefringence as great as 0.045 at the operating wavelength of 1.55 um [15].

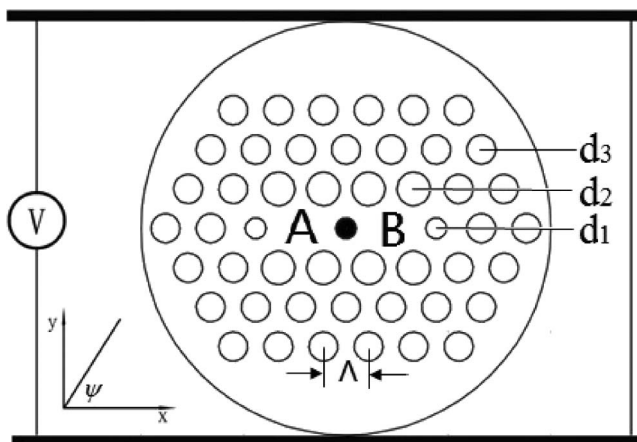


Fig. 1. Cross-section of the proposed polarization splitter in dual-core photonic crystal fiber with a liquid crystal modulation core. The insert shows the rotation angle of NLC of E7.

Polarization beam splitters are of great application value in integrated photonics circuits. Many researchers have contributed to the development of the polarization splitters. Zhang [16] reported a 1.7 mm long splitter with the splitting ratio better than  $-11$  dB and a bandwidth of 40 nm. Saitoh [17] designed a novel three-core PCF polarization splitter which is 1.9 mm long and extinction ratio better than  $-20$  dB with a bandwidth of 37 nm. The functional materials infiltrated in the air holes improve the performance of the polarization splitters. Hameed [18] demonstrated a NLC filled soft glass polarization splitter with the coupling length of 8.227 mm and bandwidths of 30 nm and 75 nm for quasi TE and TM modes, respectively. However, the PCFs in which all the air holes are infiltrated with liquid crystal suffer sharp increasing of confinement losses. Sun [19] proposed a silver wire filled polarization splitter which is 6.3 mm long and extinction ratio better than  $-20$  dB with a bandwidth of 146 nm. The PCFs with the infilling of metal wires also suffer sharp increasing of confinement losses due to the surface plasmon resonance.

In this paper, a polarization splitter based on NLC of E7 infiltrated silica glass PCF was proposed, and the polarization splitter characteristics were numerically studied by the finite element method (FEM). Only one air hole in the center of the PCFs was infiltrated with NLC of E7. The simulation results show that the polarization splitter has ultrabroad bandwidth, short coupling length, high extinction ratio and nice fabrication tolerance. The extinction ratio of the polarization splitter maintains better than  $-20$  dB at the wavelength of  $1.55 \mu\text{m}$  as the temperature increasing from  $15^\circ\text{C}$  to  $50^\circ\text{C}$ . The designed polarization splitter is a promising candidate for splitter devices.

## 2. The Novel Design of Polarization Splitter

Fig. 1 shows the cross section of the polarization splitter based on dual-core PCFs. All the air holes are placed in a triangular lattice. Two air holes are taken out to form core A and core B. The small air holes with diameters of  $d_1$  are placed at the left and right of the core A and core B. Eight big air holes with diameters of  $d_2$  are arranged above and below of the core A and core B. The outside air holes with diameter of  $d_3$  are used to confine the power in the cores. The lattice pitch is labeled by  $\Lambda$ . The dark air hole with diameter of  $d_1$  is infiltrated with NLC of E7. The lights transferring through the PCF are index guiding, due to that only one air hole in the center of the PCF is infiltrated with NLC of E7. The birefringence of the core A and core B leads to different coupling length in x-polarized direction and y-polarized direction. Thus, the polarization splitter can be realized.

The background material of the novel designed polarization splitter is silica and the dispersion relationship can be expressed by the Sellmeier equation:

$$n^2 = 1 + \sum_{j=1}^m \frac{B_j \lambda^2}{\lambda^2 - \lambda_j^2} \quad (1)$$

where  $m = 3$ ,  $B_1 = 0.6961663$ ,  $B_2 = 0.4079426$ ,  $B_3 = 0.8974794$ ,  $\lambda_1 = 0.0684043$ ,  $\lambda_2 = 0.1162414$ ,  $\lambda_3 = 9.896161$ . The Cauchy equation is used to describe the refractive indices of E7 at visible wavelengths. Li [20] extended the Cauchy equation to link the visible refractive indices to far infrared region. The ordinary index  $n_o$  and extraordinary index  $n_e$  which are used to characterize the anisotropic material of E7 can be described as follows:

$$n_o = A_o + B_o/\lambda^2 + C_o/\lambda^4 \quad (2)$$

$$n_e = A_e + B_e/\lambda^2 + C_e/\lambda^4 \quad (3)$$

where the coefficients of  $A_o$ ,  $B_o$ ,  $C_o$ ,  $A_e$ ,  $B_e$ , and  $C_e$  are sensitive to the temperature of  $T$ . The relative permittivity tensor  $\varepsilon_r$  of E7 is defined as

$$\varepsilon_r = \begin{pmatrix} n_o^2 \sin^2(\psi) + n_e^2 \cos^2(\psi) & (n_e^2 - n_o^2) \cos(\psi) \sin(\psi) & 0 \\ (n_e^2 - n_o^2) \cos(\psi) \sin(\psi) & n_o^2 \cos^2(\psi) + n_e^2 \sin^2(\psi) & 0 \\ 0 & 0 & n_o^2 \end{pmatrix} \quad (4)$$

where  $\psi$  is the rotation angle of NLC of E7.

### 3. Simulation Results and Analysis

The FEM providing high accuracy and flexible triangular meshes was implemented to characterize the designed polarized splitter. The PCF was divided into 9756 triangular meshes. The scattering boundary conditions and perfect matched layer are employed in the simulation process. According to the super modes theory, there are four super modes existing in the dual-core PCFs, including two odd modes ( $\phi_{odd}^x, \phi_{odd}^y$ ) with refractive index of ( $n_{odd}^x, n_{odd}^y$ ) and two even modes ( $\phi_{even}^x, \phi_{even}^y$ ) with refractive index of ( $n_{even}^x, n_{even}^y$ ). Fig. 2 shows the electrical field distribution of the four super modes. It should be noted that a little power transfers in the NLC modulation core. The field power percentages in the NLC modulation core are 7.2%, 0.8%, 0.5%, and 1.5% for  $\phi_{even}^x, \phi_{even}^y, \phi_{odd}^x$ , and  $\phi_{odd}^y$ , respectively. The electrical fields' energy in cores A and B are much stronger than in NLC modulation core and the operation principle of the polarization splitter can be explained by the dual-core modes coupling theory. The coupling lengths of the polarization splitter are defined as:

$$L_{x,y} = \frac{\lambda}{2(n_{even}^{x,y} - n_{odd}^{x,y})}. \quad (5)$$

The anisotropic NLC of E7 infiltrated in the central air hole leads to large birefringence, and the difference of refractive index results in different coupling lengths in two orthogonal directions. The separate length is usually common multiple of the coupling lengths in x-polarized direction and y-polarized direction. The hybrid polarization lights launched into the polarization splitter can be separated at the separate length. Fig. 3 shows the coupling lengths and coupling lengths ratio as functions of diameters of  $d_2$  (a) and adjacent air holes pitch of  $\Lambda$  (b). The wavelength is set as  $1.55 \mu\text{m}$ . It should be noted that the coupling length ratio has no significant variation and maintains at a low value of about 1.15 as changing the PCF structure parameters in no E7 infiltrated PCFs. It reveals that the separate length in no E7 infiltrated PCFs is at least several multiple of the coupling lengths. The coupling lengths in the two orthogonal directions reduce nearly one magnitude as the infilling of NLC of E7. The coupling lengths ratio in NLC of

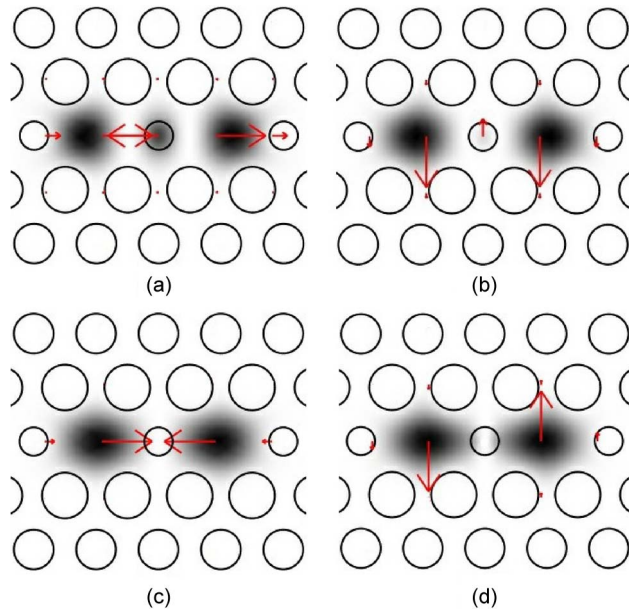


Fig. 2. Field distribution of the four super modes. (a)  $\phi_{\text{even}}^x$ , even mode in x-polarized direction, (b)  $\phi_{\text{even}}^y$ , even mode in y-polarized direction, (c)  $\phi_{\text{odd}}^x$ , odd mode in x-polarized direction and (d)  $\phi_{\text{odd}}^y$ , odd mode in y-polarized direction.

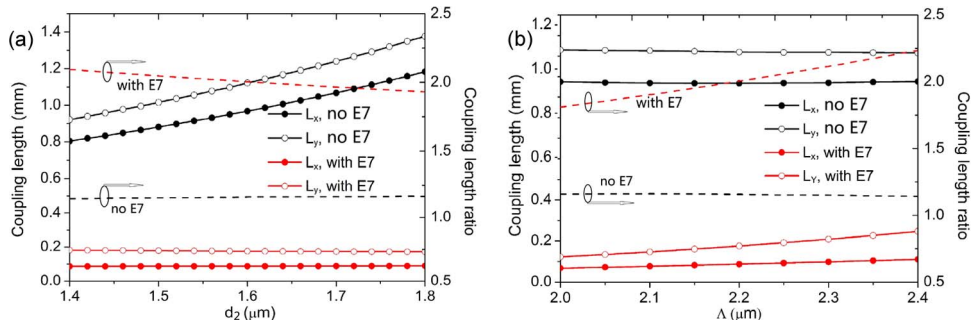


Fig. 3. Coupling lengths and coupling lengths ratio as functions of diameters of  $d_2$  (a) and adjacent air holes pitch of  $\Lambda$  (b).

E7 infiltrated PCFs experiences obvious variation as changing the diameters of  $d_2$  and adjacent air hole pitch of  $\Lambda$ . When the PCFs parameters are  $d_1 = 1.0 \mu\text{m}$ ,  $d_2 = 1.611 \mu\text{m}$ ,  $d_3 = 1.4 \mu\text{m}$ ,  $\Lambda = 2.2 \mu\text{m}$ ,  $\psi = 90^\circ$ , and  $T = 25^\circ \text{C}$ , the coupling lengths ratio reaches to 2. At this ratio, the separate length attains a value of about 0.175 mm. This is the shortest separate length being reported in polarization splitters based on PCFs, to our best knowledge. The hybrid polarization lights launched into core A can be separated into y-polarized light in B port and x-polarized light in A port at the separate length.

The initial power is launched into core A. The normalized output power of the cores A and B are calculated based on the mode coupling theory. Fig. 4 shows the output power variation along the propagation distance in the cores A (a) and B (b). One can clearly see that the lights in y-polarized direction couple to the B port completely, and meanwhile the lights in x-polarized direction go back to the A port at the separate length of 0.175 mm. The confinement losses are 0.073 dB/m, 0.018 dB/m, 0.0076 dB/m, and 0.005 dB/m for the four super modes of  $\phi_{\text{even}}^x$ ,  $\phi_{\text{even}}^y$ ,  $\phi_{\text{odd}}^x$ , and  $\phi_{\text{odd}}^y$  at the wavelength of 1.55 μm. It indicates that the designed PCFs can be used as polarization splitters.

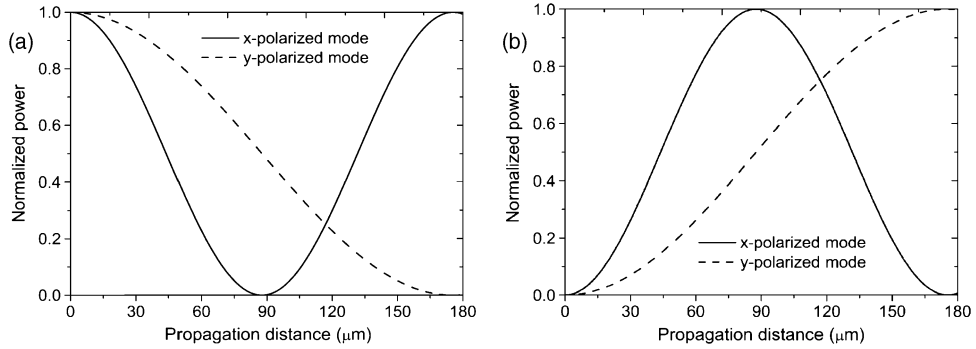


Fig. 4. The normalized output power variation along the propagation distance in core A (a) and core B (b).

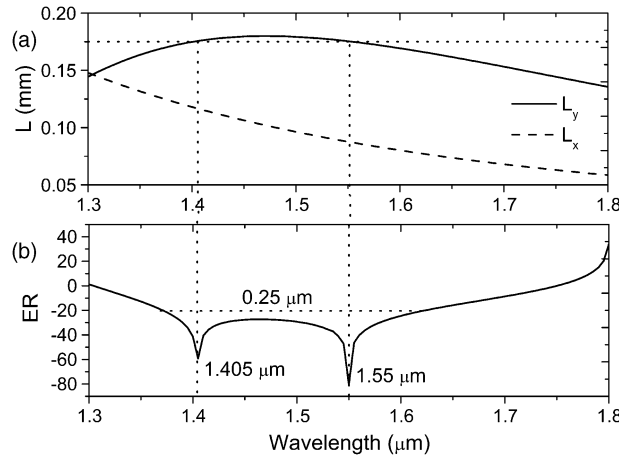


Fig. 5. (a) The coupling lengths and (b) the extinction ratio spectra. The parameters of the polarization splitter are  $d_1 = 1.0 \mu\text{m}$ ,  $d_2 = 1.611 \mu\text{m}$ ,  $d_3 = 1.4 \mu\text{m}$ ,  $\Lambda = 2.2 \mu\text{m}$ ,  $\psi = 90^\circ$ ,  $T = 25^\circ\text{C}$  and the fiber length  $L = 0.175 \text{ mm}$ .

The dispersion relationship is influenced by the light frequency. It results in the fact that the coupling lengths and extinction ratio are depending on the wavelength. The extinction ratio of ER in core A is defined as:

$$ER = 10\log_{10} \frac{P_y^A}{P_x^A} \quad (6)$$

where  $P_x^A$  is the output power in x-polarized direction and  $P_y^A$  is the output power in y-polarized direction at A output port. Broadband operating is a key factor for the application of polarization splitter. Fig. 5 shows the coupling lengths (a) and ER spectra (b) of the polarization splitter. The coupling length in y-polarized direction increases as wavelength increasing from  $1.3 \mu\text{m}$  to  $1.47 \mu\text{m}$  and decreases as wavelength increasing from  $1.47 \mu\text{m}$  to  $1.8 \mu\text{m}$ . The coupling length in x-polarized direction decreases gradually as wavelength increasing from  $1.3 \mu\text{m}$  to  $1.8 \mu\text{m}$ . From Fig. 5(b), we can see that ER reaches minimum value of  $-80.7 \text{ dB}$  at the wavelength of  $1.55 \mu\text{m}$  and secondary minimum value of  $-59.2 \text{ dB}$  at the wavelength of  $1.405 \mu\text{m}$ . The coupling length in y-polarized direction has the same value at the wavelength of  $1.55 \mu\text{m}$  and  $1.405 \mu\text{m}$  shown in Fig. 5(a). It indicates that the y-polarized lights at the wavelength of  $1.55 \mu\text{m}$  and  $1.405 \mu\text{m}$  launched into core A transfer to core B completely. The coupling length in y-polarized direction maintains an insignificant increase with no more than 3% between  $1.405 \mu\text{m}$  and  $1.55 \mu\text{m}$ . And most of the energy in y-polarized direction transfers to core B. Thus, a broadband

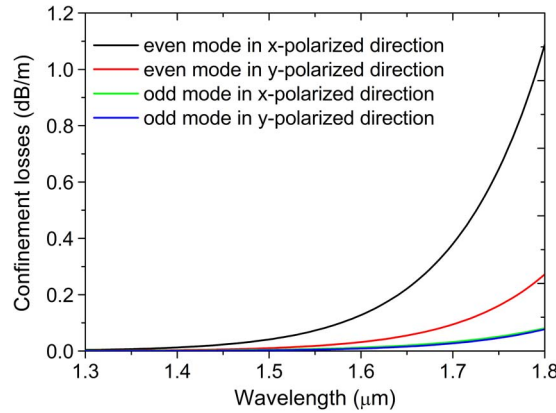


Fig. 6. The confinement losses spectra of the four super modes.

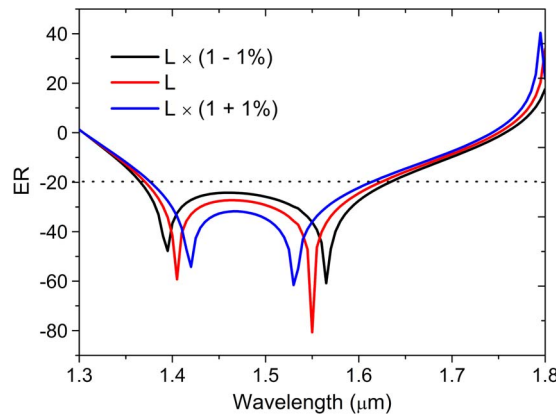


Fig. 7. The extinction ratio spectra with different fabrication tolerance of fiber length  $L$ .

bandwidth of  $0.25 \mu\text{m}$  from  $1.375 \mu\text{m}$  to  $1.625 \mu\text{m}$  with ER better than  $-20 \text{ dB}$  is obtained. It covers the E S C L optical communication bands.

Fig. 6 shows the confinement losses spectra of the four super modes. As the wavelength increasing, the confinement of the energy in the transfer cores becomes weaker and the transmission losses get larger. The energy transferring in the modulation core of E7 increases the transmission losses. The confinement loss of even mode in x-polarized direction is bigger than the others. It should be noted that the confinement losses maintain lower than  $1.2 \text{ dB/m}$  when the wavelength increasing from  $1.3 \mu\text{m}$  to  $1.8 \mu\text{m}$ . The low confinement losses make the designed PCF suitable for the polarized splitter.

Although many technologies have been introduced to fabricate PCFs currently, it is still difficult to produce PCFs with several different air holes diameters and irregular air holes precisely. Our designed polarization splitter with three different air holes diameters, none irregular air holes and low duty cycle is easy to fabricate. It is likely to control the fabrication accuracy within 1% based on the modern fabrication technology [21]. The fabrication tolerance is necessary to be analyzed in order to get a low rejection rate. Fig. 7 shows the ER spectra at different fabrication tolerance of fiber length. The fabrication tolerance of fiber length is set as 1%. The bandwidth gets larger when the fiber length decreases 1%. This is because the coupling length in y-polarized direction becomes shorter when the wavelength is greater than  $1.55 \mu\text{m}$  and less than  $1.405 \mu\text{m}$ , as shown in Fig. 5(a). The bandwidth gets narrower when the fiber length increases 1%. The ER maintains better than  $-20 \text{ dB}$  from  $1.38 \mu\text{m}$  to  $1.61 \mu\text{m}$  when the fiber length changes 1%.

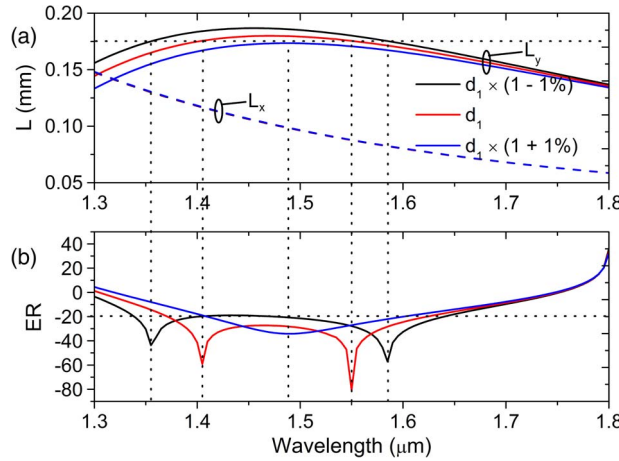


Fig. 8. (a) The coupling lengths and (b) the extinction ratio spectra with different fabrication tolerance of  $d_1$ .

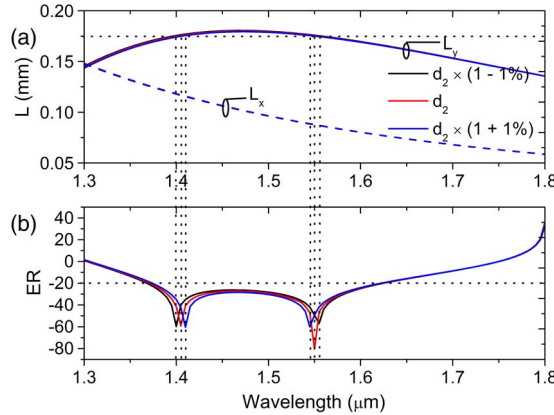


Fig. 9. (a) The coupling lengths and (b) the extinction ratio spectra with different fabrication tolerance of  $d_2$ .

The coupling lengths and ER spectra versus diameters of  $d_1$  at different fabrication tolerance are illustrated in Fig. 8. The bandwidth of ER spectra becomes larger when the diameters of  $d_1$  decreases 1%. This is own to the fact that the coupling length in y-polarized direction has significant influence on ER spectra. The difference of refractive index in y-polarized direction gets smaller when the diameters of  $d_1$  decrease. Thus, the coupling length in y-polarized direction becomes larger as shown in Fig. 8(a). On the other hand, the diameters of  $d_1$  have no significant influence on the difference of refractive index in x-polarized direction and the coupling length in x-polarized direction varies little. The ER spectrum obtains a minimum value at the wavelength of  $1.34 \mu\text{m}$  and second minimum value at the wavelength of  $1.64 \mu\text{m}$ . When the diameters of  $d_1$  get larger, the bandwidth of ER spectra becomes narrower and only one peak appears at the wavelength of  $1.49 \mu\text{m}$  as the diameters of  $d_1$  increasing 1%. The coupling lengths and ER spectra versus diameters of  $d_2$  are depicted in Fig. 9(a) and (b), respectively. It is clearly to see that the diameters of  $d_2$  have no significant influence on the coupling length in y-direction and ER spectra. The bandwidth of ER spectra becomes narrower when the diameters of  $d_2$  increase and becomes larger when the diameters of  $d_2$  decrease. The difference of refractive index in y-polarized direction gets larger when the adjacent air holes pitch of  $\Lambda$  decreases.

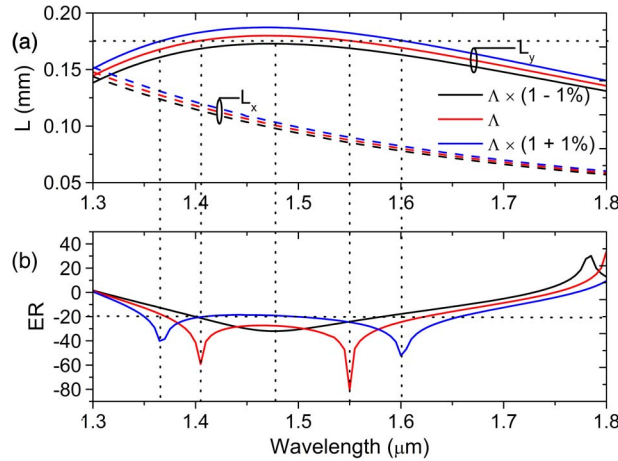


Fig. 10. (a) The coupling lengths and (b) the extinction ratio spectra with different fabrication tolerance of  $\Lambda$ .

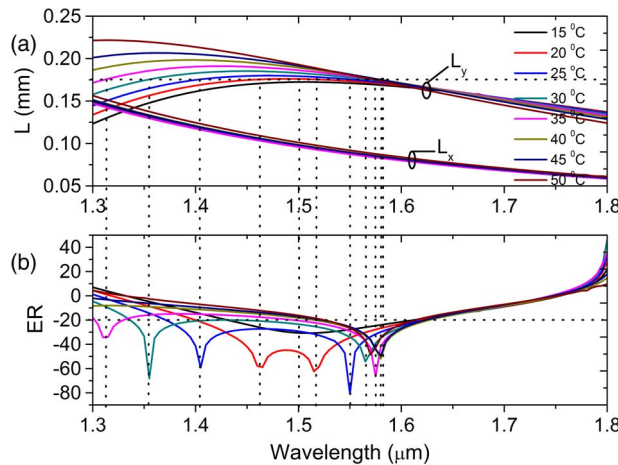


Fig. 11. (a) The coupling lengths and (b) the extinction ratio spectra with different temperature.

Thus, the coupling length in y-polarized direction becomes smaller as shown in Fig. 10(a). Fig. 10(b) shows the ER spectra with different fabrication tolerance of  $\Lambda$ . It reveals that the bandwidth of the ER spectra gets narrower when the adjacent air holes pitch of  $\Lambda$  decreases and become larger when the adjacent air holes pitch of  $\Lambda$  increases. The effects of the outside air holes with diameters of  $d_3$  are neglected as they have weak influence on the refractive index of the super modes.

The anisotropy property of NLC of E7 is influenced by the temperature. When the temperature increases from 15 °C to 50 °C, the ordinary index of E7 varies little which leads to tiny variation in coupling length in x-polarized direction. On the contrary, the extraordinary index  $n_e$  of E7 decreases remarkably which results in the increasing of the coupling length in y-polarized direction as temperature increasing from 15 °C to 50 °C. Fig. 11 shows the coupling lengths (a) and ER spectra (b) versus temperature changing from 15 °C to 50 °C. It is found that the ER maintains better than  $-20$  dB at the wavelength of  $1.55 \mu\text{m}$  when temperature increases from 15 °C to 50 °C. As the temperature is lower than 25 °C, the bandwidth of ER spectra becomes narrower. As the temperature increasing, the bandwidth gets broadened. When the temperature is higher than 30 °C, the ER becomes worse than  $-20$  dB at the E S optical communication bands and maintains better than  $-20$  dB at the C L optical communication bands.

## 4. Conclusion

In conclusion, a novel polarization splitter based on dual-core silica glass photonic crystal fiber with a liquid crystal modulation core is proposed and analyzed by the finite element method. The simulation results demonstrate that the polarization splitter has an ultrabroad bandwidth of 250 nm covering the E S C L optical communication bands with extinction ratio better than  $-20$  dB. The coupling length is 0.175 mm which is the shortest value being reported in polarization splitter based on PCFs, at our best knowledge. The extinction ratio reaches to  $-80.7$  dB at the communication wavelength of 1550 nm. The polarization splitter exhibits nice splitter performance as the fabrication deviation reaching to 1%. The extinction ratio maintains better than  $-20$  dB at the C L optical communication bands as the temperature increasing from  $15^{\circ}\text{C}$  to  $50^{\circ}\text{C}$ .

## Acknowledgement

The authors wish to thank the anonymous reviewers for their valuable suggestions.

## References

- [1] P. S. J. Russell, "Photonic crystal fibers," *Science*, vol. 299, no. 5605, pp. 358–362, 2003.
- [2] Y. Ni, L. Zhang, L. An, J. Peng, and C. Fan, "Dual-core photonic crystal fiber for dispersion compensation," *IEEE Photon. Technol. Lett.*, vol. 16, no. 6, pp. 1516–1518, Jun. 2004.
- [3] P. Zu, C. C. Chan, and W. S. Lew, "Temperature-insensitive magnetic field sensor based on nanoparticle magnetic fluid and photonic crystal fiber," *IEEE Photon. J.*, vol. 4, no. 2, pp. 491–498, Apr. 2012.
- [4] H. W. Lee, M. A. Schmidt, H. K. Tyagi, L. P. Sempere, and P. S. J. Fussell, "Polarization-dependent coupling to plasmon modes on submicron gold wire in photonic crystal fiber," *Appl. Phys. Lett.*, vol. 93, no. 11, pp. 111102, 2008.
- [5] B. Shuai, L. Xia, and D. Liu, "Coexistence of positive and negative refractive index sensitivity in the liquid-core photonic crystal fiber based plasmonic sensor," *Opt. Exp.*, vol. 20, no. 23, pp. 25858–25866, 2012.
- [6] A. Candiani, M. Konstantaki, W. Margulis, and S. Pissadakis, "A spectrally tunable microstructured optical fibre Bragg grating utilizing an infiltrated ferrofluid," *Opt. Exp.*, vol. 18, no. 24, pp. 24654–24660, 2010.
- [7] Y. Miao, B. Liu, K. Zhang, Y. Liu, and H. Zhang, "Temperature tunability of photonic crystal fiber filled with Fe<sub>3</sub>O<sub>4</sub> nanoparticle fluid," *App. Phys. Lett.*, vol. 98, no. 2, pp. 021103-1–021103-3, Jan. 2011.
- [8] W. Qian *et al.*, "High-sensitivity temperature sensor based on an alcohol-filled photonic crystal fiber loop mirror," *Opt. Lett.*, vol. 36, no. 9, pp. 1548–1550, May 2011.
- [9] A. Samoc, "Dispersion of refractive properties of solvents: Chloroform, toluene, benzene, and carbon disulfide in ultraviolet, visible, and near-infrared," *J. App. Phys.*, vol. 94, no. 9, pp. 6167–6174, 2003.
- [10] L. Rindorf and O. Bang, "Highly sensitive refractometer with a photonic-crystal-fiber long-period grating", *Opt. Let.*, vol. 33, no. 6, pp. 563–565, 2008.
- [11] J. Du *et al.*, "Electrically tunable Sagnac filter based on a photonic bandgap fiber with liquid crystal infused," *Opt. Lett.*, vol. 33, no. 19, pp. 2215–2217, Oct. 2008.
- [12] L. Xiao *et al.*, "Fabrication of selective injection microstructured optical fibers with a conventional fusion splicer," *Opt. Exp.*, vol. 13, no. 22, pp. 9014–9022, Oct. 2005.
- [13] L. Scolari *et al.*, "Continuously tunable devices based on electrical control of dual-frequency liquid crystal filled photonic bandgap fibers," *Opt. Exp.*, vol. 13, no. 19, pp. 7483–7496, Sep. 2005.
- [14] L. Wei *et al.*, "Continuously tunable all-in-fiber devices based on thermal and electrical control of negative dielectric anisotropy liquid crystal photonic bandgap fibers," *Appl. Opt.*, vol. 48, no. 3, pp. 497–503, Jan. 2009.
- [15] M. F. O. Hameed and S. S. A. Obayya, "Modal analysis of a novel soft glass photonic crystal fiber with liquid crystal core," *J. Lightw. Technol.*, vol. 30, no. 1, pp. 96–102, 2012.
- [16] L. Zhang and C. Yang, "Polarization splitter based on photonic crystal fibers," *Opt. Exp.*, vol. 11, no. 9, pp. 1015–1020, May 2003.
- [17] K. Saitoh, Y. Sato, and M. Koshiba, "Polarization splitter in three-core photonic crystal fiber," *Opt. Exp.*, vol. 12, no. 17, pp. 3940–3946, 2004.
- [18] M. F. O. Hameed, and S. S. A. Obayya, "Polarization splitter based on soft glass nematic liquid crystal photonic crystal fiber," *IEEE Photon. J.*, vol. 1, no. 6, pp. 265–276, Dec. 2009.
- [19] B. Sun, M. Y. Chen, J. Zhou, and Y. K. Zhang, "Surface plasmon induced polarization splitting based on dual-core photonic crystal fiber with metal wire," *Plasmonics*, vol. 8, no. 2, pp. 1253–1258, Jun. 2013.
- [20] J. Li, S. T. Wu, S. Brugioni, R. Meucci, and S. Faetti, "Infrared refractive indices of liquid crystals," *J. Appl. Phys.*, vol. 97, no. 7, pp. 073501, Apr. 2005.
- [21] W. Lu, S. Lou, X. Wang, L. Wang, and R. Feng, "Ultrabroadband polarization splitter based on three-core photonic crystal fibers," *Appl. Opt.*, vol. 52, no. 3, pp. 449–455, Jan. 2013.